Original Research

Exploring the role of phospholipid membrane composition in biomolecular simulations: towards tailored membrane models

Marco Cavaglià*, Silvia Vernuccio, Jack A.Tuszynski.

Department of Mechanical and Aerospace Engineering (DIMEAS), Bioengineering Group, Polytechnic University of Torino, I-10129 Turin, Italy.

***Correspondence**: marco.cavaglia@polito.it
DOI: https://doi.org/10.56280/1702405472

Received: 29 May 2025 Accepted: 26 June 2025 Online Published: 28 June 2025

Abstract

Cell membranes are highly complex biological systems composed of a wide array of lipid species, distributed asymmetrically across the bilayer leaflets. This highly specific lipid composition is crucial for maintaining membrane integrity and functionality; however, simplified models are often employed in molecular dynamics (MD) simulations. Such simplifications may lead to inaccurate representations of the membrane's structural and functional characteristics. In this study, we compare a generic mammalian membrane model with two brain-specific neuronal membrane models to assess the impact of lipid composition on simulation outcomes. By combining experimental data and earlier computational models, we developed consensus models representing the membrane of the neuronal soma and the synaptic plasma membrane, using lipids with readily available and validated molecular mechanics parameters in the CHARMM36 force field. MD simulations revealed distinct structural and mechanical properties in brain-specific membranes, including increased area per lipid, reduced membrane thickness, and lower bending stiffness, compared to generic membranes. These differences are expected to influence the behavior of embedded proteins and the membrane's response to electrochemical signals, underscoring the functional significance of lipid diversity. In particular, the bending modulus K_c was markedly reduced in brain-specific models (K_c=51.47 kBT and K_c=47.87 kBT for soma and synaptic membranes, respectively) compared to the average mammalian cell membrane model (K_c=89.80 kBT), reflecting increased membrane flexibility. These findings underscore the importance of utilizing tissue-specific membrane models to obtain biologically accurate insights in MD simulations.

Keywords: molecular dynamics, molecular models, cell membranes, membrane mechanics, lipid composition, neuronal membranes, electrostatics.

1. Introduction

The cellular plasma membrane is a dynamic barrier composed of a complex lipid and protein network, determining the physical and functional capabilities of the cell. The variety of lipids composing the membrane varies significantly across different cell types, submembrane compartments, organelles, and is profoundly influenced by developmental stages, tissue types, environmental factors, and pathological states (Harayama & Riezman, 2018). In neuronal cells, for instance, the membrane's lipid composition is specifically tailored for maintaining cellular signaling and neuronal connectivity (Wilson et al., 2020). In recent years, the study of neuronal membranes has acquired significant interest within the field of computational neuroscience and molecular modelling, due to the critical role these membranes play in cellular signaling and overall brain function. The lipid composition and diversity within the membrane is particularly relevant in modulating its physical properties and its interactions, which is especially pronounced in neuronal membranes, is not merely a passive attribute, but constitutes a biophysical characteristic which actively participates in cellular signaling by influencing protein activity, e.g., ion channel dynamics (Ponaro & Lolicato, 2022; Tillman & Cascio, 2003; Cordero-Morales & Vásquez, 2018), and synaptic functions. Such heterogeneity arises from the presence of various lipid types, including phospholipids, cholesterol, and glycolipids, all of which establish dynamic interactions crucial for neuronal function (Westra et al., 2021; Ramos-Martín & D'Amelio, 2022). These interactions determine, for example, the membrane's asymmetry and curvature, which are essential for processes such as vesicle formation, fusion, and the proper functioning of membrane-bound proteins (Xie et al., 2023).

In the context of molecular dynamics (MD) simulations, however, the commonly employed computational models have traditionally simplified the diversity of lipid species to a few representative lipid types (and, at

Journal of Multiscale Neuroscience

times, even reducing membranes to single-component phosphatidylcholine lipid bilayers), potentially overlooking critical aspects of membrane behavior and structure that emerge from complex lipid interactions (Marrink et al., 2019). Recent advances in computational methods and increased understanding of lipidomics have allowed for more detailed and accurate representations of membrane composition and dynamics. Such models are crucial for elucidating, for example, the mechanistic underpinnings of neurophysiological processes, including the etiology of neuropathological conditions where membrane composition is disrupted (Grassi et al., 2020; Mesa-Herrera et al., 2019; Kao et al., 2020) and general anesthetic pharmacodynamics (Rehberg et al., 1995; Miller & Pang, 1976; Hantal et al., 2019; Rózsa et al., 2023). Indeed, alterations in lipid composition have been associated with a variety of neurological conditions, such as Alzheimer's Disease and other neurodegenerative disorders, where lipid imbalances can disrupt cellular homeostasis and worsen disease progression (Mesa-Herrera et al., 2019). The complexity of these interactions and their implications for disease are beginning to be decoded through more realistic computational models, which incorporate the diverse lipid types experimentally identified in specific neuronal compartments (Yoon et al., 2022).

In this work, we investigate how variations in lipid composition affect the geometrical, structural, and mechanical characteristics of lipid bilayers in MD simulations. We compare simplified membrane models commonly used in the literature with membrane compositions that more closely reflect the complexity of neuronal membranes. By incorporating recent experimental data on neuronal lipidomics, we construct all-atom membrane models using publicly available parameters and tools, offering a more accurate representation of the physical, dynamic and chemical properties of neural membranes. Through a comparative analysis of structural and dynamical properties across various membrane compositions, our findings reveal both important similarities and key differences. These differences highlight the unique regulatory roles of lipids, particularly in the context of neuronal pathophysiology. This approach not only advances the understanding of the structure-to-function relationships in membranes but also highlights the importance of selecting appropriate membrane models in MD studies, particularly when investigating membrane-associated receptors and channels (Dias & Nylandsted, 2024), in the context of neuroscience and drug development.

2. Molecular dynamics (MD) simulations

Molecular dynamics (MD) simulations of the constructed membrane models were performed as follows: the simulation protocol consisted of an initial energy minimization to relax the system using the steepest descent algorithm (Hess et al., 2008; Van Der Spoel et al., 2005) for a maximum of 5000 steps or until the maximum force on atoms dropped below 1000 $kJ \cdot mol^{-1} \cdot nm^{-1}$. Subsequently, six steps of system equilibration were carried out following the suggested CHARMM-GUI protocol: the first three steps of equilibration were performed for 125 ps each in the canonical (NVT) ensemble, with a conservative timestep of 1 fs and using the Berendsen thermostat set at 303.15 K and a coupling time constant of 1 ps. Subsequently, a further three steps of equilibration were performed for 500 ps each in the NPT ensemble, with a timestep of 2 fs, using the Berendsen thermostat with 303.15 K as reference temperature and 1 ps coupling time constant, and the Berendsen barostat (Berendsen et al., 1984) with 1 atm as reference pressure, 5 ps as coupling time constant, and semi-isotropic pressure coupling. After this equilibration phase, the position restraints were lifted, and production MD simulations were carried out in the NPT ensemble with a duration of 1 µs each with a 2 fs timestep, using the Nosé–Hoover thermostat (Nosé, 1984) with 303.15 K as reference temperature and 1 ps coupling time constant, and the Parrinello–Rahman barostat (Parrinello & Rahman, 1981) with 1 atm as reference pressure, 5 ps as coupling time constant, and semi-isotropic pressure coupling. The Particle Mesh Ewald algorithm was employed to calculate long-range interactions in the system, utilizing a 1.2 nm cutoff. Van der Waals interactions were cut-off at 1.2 nm, with a force-switch modifier at 1.0 nm. Bonds involving hydrogen atoms were constrained using the LINCS algorithm (Hess et al., 1997). All simulations were carried out using GROMACS version 2022.6 (Abraham et al., 2015). Visualizations of the molecular systems were created using the Visual Molecular Dynamics (VMD) software package (Humphrey et al., 1996).

2.1. Geometric, structural and mechanical analysis.

Before analyzing the data, we assessed simulation convergence by inspecting the potential energy during the energy minimization phase and by checking the distribution and time evolution of the system temperature and density. Periodic boundary conditions

(PBCs) were removed using the gmx trjconv tool wherever necessary. For all subsequent analyses, the first 250 ns of the trajectory were considered as additional structural equilibration of the systems and discarded. We then calculated the following properties of interest: (a) the area per lipid, (b) the bilayer thickness, (c) membrane density profiles, (d) lipid lateral diffusion behaviour, and (e) membrane bending modulus. The area per lipid and the bilayer thickness were calculated using in-house Python scripts relying on the MDAnalysis library (Michaud-Agrawal et al., 2011). In greater detail, the geometric area per lipid was obtained by dividing the area of the simulation box, calculated in the xy plane, by the number of lipids in a leaflet (256). Bilayer thickness was calculated as the distance between two xy planes fitted on the two point-clouds of the phosphorus atoms of the lipid heads in the two leaflets. Conversely, the densities of the different membrane subcomponents (lipid headgroups, glycerol groups, fatty acid tails, and cholesterol) were calculated at different points along the z coordinate using the gmx density tool. The lipid lateral diffusion coefficient was calculated from the mean square displacement (MSD) of the individual lipids using the gmx msd tool. In greater detail, we chose the phosphorus atoms as the reference atom for the calculation of the displacement and obtained the lateral diffusion coefficient of the lipids from the linear fit of the MSD vs. reference time in its linear region.

Finally, in addition to geometric and structural parameters, we calculated the bending modulus Kc, as a direct measure of the mechanical characteristics of the membrane, following the methodology proposed by Johner et al. (2016). Specifically, we employed Python scripts relying on the OpenStructure computational framework (Biasini et al., 2013; Biasini et al., 2010), as described in our previous work (Zizzi et al., 2022) and in the original publication.

2.2. Quantification and statistical analysis

For a more robust estimation of the uncertainties of the calculated quantities, we performed block averaging as reported in earlier literature for analogous molecular systems (Zizzi et al., 2022; Shahane et al., 2019), as follows: the 750 ns of the equilibrium portion of the production MD trajectories were divided into three 250-ns blocks, corresponding to the following time intervals: 251–500 ns, 501–750 ns, and 751–1000 ns. Then, the structural parameters and bending moduli were calculated separately for each trajectory block. This choice was made to increase the statistical robustness of the reported data, since the high correlation between consecutive frames in molecular dynamics simulations results in the underestimation of uncertainties, as exhaustively explained by Grossfield et al. (2018). By dividing the trajectory into large enough blocks, the quantities between the various blocks become uncorrelated, and from a statistical point of view, the error is estimated more robustly (Grossfield et al., 2018; Flyvbjerg & Petersen, 1989; Nicholls, 2014). Starting from these observations and following the same procedure performed by Zizzi et al. (2022), for each trajectory block, we calculated the values of the parameters of interest for each frame and then averaged them within the block using the following:

$$\bar{\mu}_j = \frac{1}{N_b} \sum_{i=1}^{N_b} p_i \quad (1)$$

where p is the structural parameter of interest, N_b is the number of frames that form a block of a) trajectory and $\bar{\mu}_j$ is the mean of p for the block of trajectory j. Then, to obtain the ensemble average <μ>, the mean of all $\bar{\mu}_j$ was calculated using the following:

$$\langle \mu \rangle = \frac{1}{n} \sum_{j=1}^{n} \bar{\mu}_j \quad (2)$$

where n is the number of blocks of trajectory (in our case, n=3). To obtain the experimental standard deviation of the mean the following was used:

$$\overline{\sigma_\mu} = \sqrt{\frac{\sum_{j=1}^{n} (\bar{\mu}_j - \langle \mu \rangle)^2}{n-1}} \quad (3)$$

where $\bar{\mu}_j$ is the mean of the parameter of interest p for a single trajectory block (calculated using eq. 1), <μ> is the mean of all mean values and n is the number of blocks of trajectory. Then, the estimate of the standard deviation was calculated using: $\sigma_\mu = \frac{\overline{\sigma_\mu}}{\sqrt{n}}$.

This quantity was used to extract the 95% confidence interval that is reported along with the quantities of interest.

3. Results

We investigated and compared the structural and dynamical behavior of three distinct phospholipid membrane compositions, one already employed in pre-

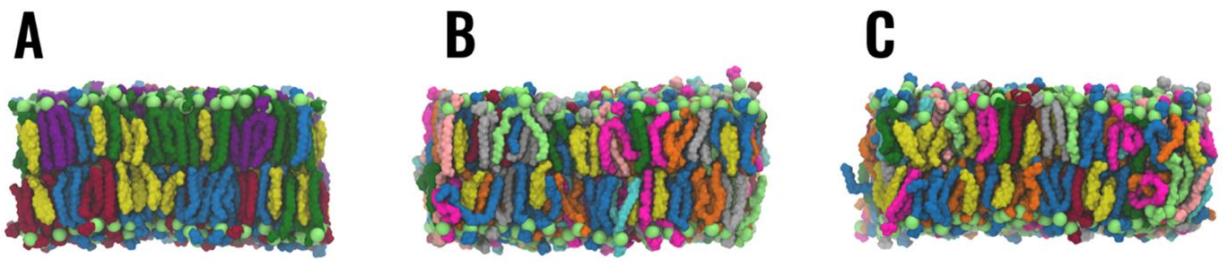

Figure 1. *The membrane of the mammalian cell used as control model (**A**), the neuronal soma membrane model (**B**) and the synaptic plasma membrane (**C**). In the images, POPC is dark blue, POPE is dark green, POPS is dark purple, PSM is dark red, cholesterol is yellow, POPI is cyan, DPPC is grey, DOPC is rose, PAPC is magenta, PAPE is orange, PAPS is lime. Phosphate heads highlighted in light green. Water and ions omitted for clarity.*

vious works and representing an average mammalian membrane, and two novel compositions representative of the neuronal soma membrane and the synaptic membrane. Our objective was to assess how using a generic membrane model versus a composition tailored to a specific tissue or organ influences the outcomes of MD simulations. The materials and methods are given in the *Appendix*. Snapshots of the simulated membrane patches are shown in **Figure 1**.

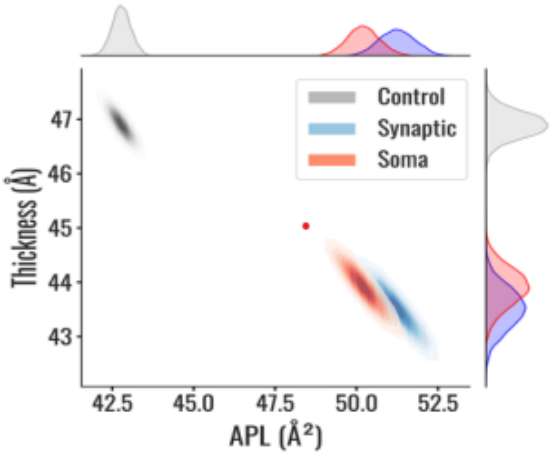

Figure 2. *Distributions of the geometric area per lipid and bilayer thickness for the membrane used as the control model (grey), for the neuronal soma membrane (red), and the synaptic plasma membrane (blue).*

3.1 Area per lipid and bilayer thickness

The area per lipid and the bilayer thickness are two quantities that characterize the structural and geometrical behavior of the simulated bilayers, and that allow for a first direct comparison with many membrane models investigated through MD simulations, as well as experimentally in the literature. Understanding the area per lipid is crucial as it influences lipid mobility within the membrane, the packing of lipid acyl chains, and the membrane's elastic properties.

Table 1. *Mean values for the gAPL and thickness of the membrane models. The first row reports the mean values for the corresponding quantities in the mammalian cell membrane model from a previous study (Zizzi et al., 2022). 95% CIs after block averaging are reported in square brackets.*

System	gAPL [Å²]	Bilayer Thickness [Å]
Previous work	42.89 [42.83-42.95]	46.85 [46.81-46.89]
Mammalian	42.78 [42.75-42.81]	46.90 [46.88-46.92]
Soma	50.21 [50.18-50.24]	43.91 [43.89-43.93]
Synaptic	51.25 [51.23-51.27]	43.52 [43.50-43.54]

The mean value of the area per lipid for the neuronal soma membrane and for the synaptic plasma membrane were 50.21 Å² (95% CI: 50.18–50.24 Å²) and 51.25 Å² (95% CI: 51.23–51.27 Å²) respectively. These values are higher compared to the control model which showed a mean value of 42.78 Å² (95% CI: 42.75–42.81 Å²). The mean membrane thickness for the neuronal soma membrane was 43.91 Å (95% CI: 43.89–43.93 Å), whereas the synaptic plasma membrane featured a mean thickness of 43.52 Å (95% CI: 43.50–43.54 Å). Both values were found to be lower compared to the control model (46.90 Å [46.88–46.92 Å]). As expected, the mean area per lipid and membrane thickness of the control model nicely replicated the corresponding results obtained for the same membrane composition in a previous study (Zizzi et al., 2022) (42.89 Å² and 46.85 Å, respectively). Data

Table 2. *Mean values of lipid lateral diffusion coefficients with 95% CIs for each phospholipid and cholesterol. The last column reports the global average value for all the calculated lateral diffusion coefficients.*

System	POPC	POPE	POPS	POPI	PAPC	PAPE	PAPS	DOPC	DPPC	PSM	CHOL	AVG
Control	1.08 [0.86-1.30]	1.14 [0.95-1.33]	1.12 [0.90-1.34]	/	/	/	/	/	/	0.97 [0.80-1.14]	1.10 [0.90-1.30]	1.08 [1.07-1.09]
Soma	4.10 [3.88-4.32]	3.94 [3.58-4.30]	/	4.13 [3.87-4.39]	4.09 [3.95-4.23]	3.89 [3.77-4.01]	4.01 [3.53-4.49]	3.99 [3.57-4.41]	4.05 [3.85-4.25]	3.92 [3.38-4.46]	4.03 [3.85-4.21]	4.01 [4.00-4.02]
Synaptic	4.15 [3.91-4.39]	4.22 [3.90-4.54]	/	4.16 [3.96-4.36]	4.41 [4.22-4.60]	4.75 [4.47-5.03]	3.96 [3.61-4.31]	4.46 [3.91-5.01]	4.15 [3.92-4.38]	3.71 [3.38-3.94]	4.25 [4.11-4.39]	4.22 [4.20-4.24]

regarding area per lipid and bilayer thickness are summarized in **Table 1**.

Considering the two brain-specific membrane models, the previous computational study, which we considered for choosing their lipid tail compositions (Ingólfsson et al., 2017), reported a mean gAPL of 46.0 Å² for the outer leaflet and 48.5 Å² for the inner leaflet, and an average membrane thickness of 40.57 Å. The brain-specific membranes simulated herein showed comparable gAPL and thickness values, consistent with the similar lipid composition. Conversely, considering the generic mammalian membrane model, the comparison with previous work (Zizzi et al., 2022) simulating the same membrane composition highlights how in molecular simulations (**Table 1**) changing the total number of lipids, i.e., changing the size of the lipid patch while maintaining the same lipid composition results in negligible differences in area per lipid (42.89 vs. 42.78 Å²) and membrane thickness (46.85 vs. 46.9 Å). Conversely, altering the membranes' lipid composition resulted in more substantial changes, specifically an increase in the area per lipid and a decrease in membrane thickness when comparing generic and brain-specific models. Our results thus show how the choice of the specific lipids to include in the computational membrane model, and their relative ratios, results in remarkable changes in the structural properties of the membrane, suggesting how choosing the correct lipid types and ratios based on the tissue type relevant for the system under investigation may substantially affect the results obtained from MD simulations. Interestingly, no substantial differences in the gAPL and the membrane thickness were observed between the two brain-specific membrane models, namely the neuronal soma membrane and the synaptic membrane (gAPL: 50.21 Å² vs 51.25 Å²; thickness: 43.91 Å vs. 43.52 Å, respectively), coherently with the very similar lipid composition between the two models and the similar cholesterol content.

In summary, we confirmed that membrane composition has a significant impact on the geometrical equilibrium reached by the computational membrane models, consistent with previous findings that highlight the effect of membrane composition on bilayer thickness (Li et al., 2012). In this regard, the presence and amount of cholesterol is particularly relevant: the ordering effect of cholesterol straightens the fatty acid chains of lipids, reducing steric repulsion and thus decreasing the area per lipid while increasing the membrane thickness. In the present work, the brain-specific membranes contained fewer cholesterol molecules than the control model (see **Figure 2**), and thus exhibited increased area per lipid and decreased bilayer thickness. In general, the membranes with higher cholesterol content showed a reduction in the area per lipid and an increase in membrane thickness.

3.2 Density distributions

When examining the density distribution of the different subcomponents of the membranes (headgroups, lipid tails, glycerol moieties and cholesterol molecules), distinct patterns could be observed and are reported in **Figure 3**.

The distributions confirm how cholesterol typically positions itself between the phospholipid headgroups and the membrane core, forming a characteristic two-peak pattern. This pattern was more pronounced in the control model due to its higher cholesterol content. Furthermore, the brain-specific membranes exhibited a higher density of lipid tails at the bilayer core, in contrast with the control membrane. This increase in density is attributed to the lower cholesterol content in the brain-specific membranes, which also results in a thinner membrane. The reduced thickness and higher van der Waals attraction between the leaflets increase the density at the bilayer core (Klähn & Zacharias, 2013).

3.3 Lipid lateral diffusion

The lipid lateral diffusion behavior represents the lipids' ability to move laterally within the membrane plane. The lipid lateral diffusion coefficients obtained from our simulations are reported in **Table 2** with the 95% CIs after block averaging.

Our results highlight how all lipid types within the same membrane model typically show similar diffusion rates. When comparing the different models, the brain-specific membranes exhibited an overall faster lipid diffusion (i.e., higher diffusion coefficients) compared to the control model, likely due to their increased area per lipid resulting from the lower cholesterol content, which facilitates lipid mobility. The lateral diffusion rates obtained for the neuronal soma and synaptic plasma membrane are in agreement with literature data (Ingólfsson et al., 2017), confirming the quality of these models in replicating brain-specific membrane properties.

3.4 Membrane bending modulus

The bending modulus (K_c) calculated for the membrane models is indicative of the membrane's mechanical behavior. The mean values of K_c obtained for the different membranes of interest are reported in **Table 3**.

A direct comparison of the bending moduli (K_c) calculated from our simulations is shown in **Figure 4**. The plot also includes the bending modulus obtained in a previous study of our lab (Zizzi et al., 2022) of a mammalian membrane model with the same lipid composition as the control model simulated herein.

The neuronal soma and synaptic membrane are predicted to have a lower bending modulus than the control model, confirming how differences in lipid composition, and in particular in cholesterol content, substantially impact membrane flexibility, in agreement with current literature (Chakraborty et al., 2020; Arriaga et al., 2017; Song & Waugh, 1993; Park et al., 2022).

Table 3. *Mean K_c values for control, neuronal soma, and the synaptic plasma membrane obtained from the MD simulations. The table also reports the mean value of the bending modulus for the control mammalian cell membrane published in our previous study (Zizzi et al.,2022). 95% CIs are reported in square brackets.*

System	K_c [K_bT]
Previous Work	88.80 [87.16-90.44]
Control	89.80 [88.67-90.93]
Soma	51.47 [50.63-52.40]

Moreover, a clear difference in the bending modulus also emerged between the two neuronal membranes (51.47 kBT [95% CI: 50.63-52.40] vs 47.87 kBT [95% CI: 47.68-48.06] for the soma and synaptic membrane, respectively). Notably, altering the total number of lipids without changing the composition did not considerably affect K_c values, as can be seen from the comparison between the control model, consisting of 512 lipids, and the results from earlier work employing an 800-lipid patch with the same composition.

In contrast, altering the composition of the membrane in terms of lipid types and relative amounts led to remarkable differences in Kc. This further supports the conclusion that selecting the proper membrane composition in molecular modeling studies, especially when performing MD simulations, has a significant impact on membrane geometry and behavior. Conversely, simulating a larger or smaller membrane patch, given a fixed lipid composition, has a negligible impact. Overall, in the present work, we confirm that the type and amount of lipids and cholesterol in the membrane influence how tightly lipid molecules pack together and how easily they can move. These properties affect the thickness, density, lateral diffusion behavior and flexibility of the membrane, which are crucial factors determining its functions and interactions with other cellular components. When building molecular models of lipid bilayers for molecular simulations, the choice of specific lipid composition has substantial effects on membrane behavior, even within the constraints of only including lipids for which molecular mechanics parameters are

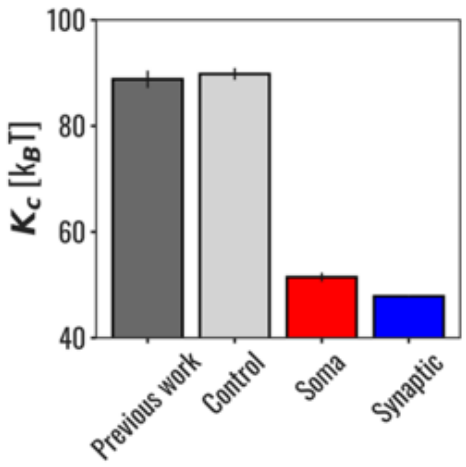

***Figure 3**. Mean values of the K_c for the control membrane, for the neuronal soma membrane, and the synaptic plasma membrane. For comparison, the mean values of K_c obtained for a mammalian membrane in our previous study are shown in dark grey.*

readily available in the literature and through online tools such as CHARMM-GUI.

4. Discussion

Cell membranes are complex biological systems, characterized by a heterogeneous composition of up to a hundred different lipid species, asymmetrically distributed across the bilayer leaflets. This highly tailored lipid distribution is essential for maintaining membrane structural integrity and functionality. However, in the context of molecular dynamics simulations, the use of highly simplified or even single-component bilayer models remains widespread, and such models may fail to capture the complexity of biological membranes. In this work, we demonstrate how changes in membrane composition can lead to significantly different results in molecular simulations by comparing a generic mammalian membrane model from previous studies (Zizzi et al., 2022) with more sophisticated, brain-specific membrane models. Our study suggests that assembling and simulating computational models of membranes that more closely mimic the composition of the tissue or cell type under investigation can lead to more biologically relevant insights. Unfortunately, the precise composition of the plasma membrane for each cell phenotype or tissue is often elusive, largely due to the current limitations of experimental techniques that allow for highly accurate membrane lipidomic profiling.

The present work specifically investigated the lipid compositions of neuronal membranes. By combining results from earlier experimental studies and computational molecular models, we developed consensus models for neuronal soma and synaptic plasma membranes, employing lipids with readily available molecular mechanics parameters. This approach enabled us to investigate the effect of membrane composition on simulation results and provided insight into how brain-specific membranes differ from those of average mammalian cells. Through MD simulations, we examined the structural and mechanical properties of these membranes. Our findings suggest that tissue-specific membrane models, such as our brain-specific membrane models, exhibit distinct characteristics, including a higher area per lipid, reduced membrane thickness, and lower bending stiffness compared to a generic membrane model. Such traits can influence the conformational behavior of embedded proteins, such as ion channels, and thus impact the response of the membrane to electrochemical signals, potentially affecting neuronal communication. By comparing our results with earlier findings (Zizzi et al., 2022), we validated the robustness of the employed simulation protocols and gained new insights into the structural and mechanical properties of brain-specific membrane models compared to generic models. These conclusions regarding the pivotal role of lipid composition in determining membrane properties underscore the complexity of the biophysical landscape of phospholipid bilayers, highlighting the importance of constructing, validating, and utilizing increasingly complex bilayer models in molecular simulations.

We demonstrate that these models can be assembled using lipid types with freely available molecular mechanics parameters in tools such as CHARMM-GUI (Jo et al., 2007, 2008, 2009; Wu et al., 2014). When information regarding the specific lipid composition of the cell or tissue under investigation is available, it is advisable to employ a bilayer model explicitly accounting for such specificity. Indeed, simpler models, such as single-lipid membrane models (e.g., a DOPC patch), may lead to a different exploration of the phase space during molecular dynamics (MD) simulation, potentially yielding substantially divergent results (Shahane et al., 2019). Among compositional factors, cholesterol emerged to be particularly relevant, further underscoring the importance of accurate lipid representation (Sok, 1999; Kozłowska et al., 1999; Róg et al., 2009; Klähn & Zacharias, 2013).

Data reported in the present work also showed a considerable difference in mechanical parameters between brain-specific and generic membrane compositions. For instance, the bending modulus Kc was lower in brain-specific models (K_c = 51.47 kBT and K_c = 47.87 kBT for soma and synaptic membranes, respectively) compared to the average mammalian membrane (K_c = 89.80 kBT). This reduction in K^c, indicative of increased membrane flexibility, has profound implications for the dynamic behavior of both membranes and their embedded proteins and biomolecules, linking mechanical properties to functional capabilities.

5. Conclusion

In this study, we investigated the biophysical and structural characteristics of biological membranes, focusing on their nanometric electric field distribution, asymmetry, and phase behavior. By integrating high-resolution molecular dynamics simulations with theoretical modeling, we characterized the distribution of electric dipoles across lipid bilayers and the emergence of surface charge differentials under physiological conditions.

Table 4. *The lipid composition of the asymmetrical lipid membrane of the mammalian cell replicated from our previous study.*

Lipid	Inner leaflet	Outer leaflet	Total
POPC	26	68	94
POPE	85	22	107
POPS	52	5	57
PSM	6	74	80
CHOL	87	87	174

Our results demonstrate that membrane asymmetry—especially the enrichment of phosphatidylserine and sphingomyelin in distinct leaflets—plays a critical role in establishing stable dipolar configurations and localized electrostatic potentials. The simulations further revealed how these charge distributions are modulated by cholesterol content and interfacial hydration layers. Moreover, we observed that under specific energetic thresholds, lipid membranes may transition into metastable phase regimes with heightened susceptibility to external perturbations.

These findings reinforce the view that lipid membranes are not passive structural barriers, but electrically active surfaces capable of dynamic reorganization and environmental responsiveness. Importantly, the study underlines the need for tissue-specific membrane models in biomolecular simulations, especially when experimental lipidomic data are available. Future work should focus on refining these models, parametrizing additional lipid species, and exploring their interactions with external electromagnetic fields—an essential step toward understanding electrosensitive biological processes at the nanoscale.

Appendix

The methods for determining each membrane composition are reported below. We extracted the specific lipid composition of the membrane of the neuronal soma and of the synaptic membrane from experimental studies available in the literature, with the aim of building molecular models that more accurately reflect the lipid profile of these two neuronal compartments. Conversely, the generic membrane model reflecting the average composition of a mammalian cell membrane was adapted from prior work (Zizzi et al., 2022).

A1. Average mammalian membrane (control model)

The first membrane model, referred to as the control model, replicates a composition investigated in a previous study from our lab (Zizzi et al., 2022). This model consisted of a composite asymmetrical lipid bilayer designed to represent an average mammalian cell membrane. It contained 800 total lipids: 1-palmitoyl-2-oleoyl-sn-glycero-3-phosphocholine (POPC), 1-palmitoyl-2-oleoyl-sn-glycero-3-phosphoethanolamine (POPE), 1,2-palmitoyl-oleoyl-sn-glycero-3-phosphoserine (POPS), Palmitoylsphingomyelin (PSM) and cholesterol (CHOL). For the present study, we created a rescaled version of this model consisting of a total of 512 lipids maintaining the same lipid types and relative abundances. The final lipid composition is reported in **Table 4**. This control model serves as the benchmark for comparing the results of the other two membrane compositions.

A2. Neuronal soma

The composition of the neuronal soma membrane model was derived from dorsal root ganglia (DRG) cells of embryonic rat pups at day 15 of their development published by Calderon et al. (1995). The study determined and reported the percentages of sphingomyelin (SM), phosphatidylcholines (PC), phos-

phatidylethanolamines (PE), inositol phospholipids, phosphatidylserine (PS), cerebrosides (CB), sulfatides (Sulf), cholesterol (CHL), cholesterol esters, triacylglycerols and fatty acids. For building a simplified molecular model containing only the dominant lipid classes, we retained only the PC, PE, PS, PI, SM headgroups and CHL, and recalculated the relative abundances after excluding the neglected lipids.

Indeed, since the focus of this work was to create a simplified all-atom model consisting of publicly available molecular mechanics parameters that would not require ad-hoc parametrization, we neglected cerebrosides, sulfatides, cholesterol esters and triacylglycerol, because of their very limited abundance in the investigated membranes. Free fatty acids were neglected because their experimental detection might also have arisen from their presence in the cytoplasm of cells, rather than in the membrane alone. Lastly, our analysis omitted the unidentified lipids in the reported work.

A3. Synaptic membrane

The composition of the synaptic membrane model was derived from presynaptic and postsynaptic membranes and synaptic thickening of nerve endings or synaptosomes of rats published by Cotman et al. (1969). Also in this case, with the rationale of constructing a simplified molecular model, we only retained the most abundant lipid headgroups, i.e. PC, PE, PS, PI, SM, and CHL. Curiously, in the above-mentioned work, only the combined percentage composition of PS and PI was reported as a single value (reported as "PI+PS"). Since no further information was reported regarding the relative abundance of these two headgroups, we assumed a 50:50 ratio of PS and PI. Ceramides, the glycolipid fraction, and lysophosphatidylcholine were neglected because of their very limited relative abundances (below 2%, leading to less than 5 lipid molecules per leaflet in a 512-lipid membrane patch).

A4. Determination of fatty acid tails for neuronal membranes

After the pre-processing and filtering of the lipids as reported above, the final percentages of the lipid classes were rescaled to 100% after removing excluded lipids to preserve their relative abundance. The final percentage compositions of the membrane models specific to the brain are shown in **Table 5.**

Table 5. *The percent compositions of different lipid classes considered for the neuronal soma membrane and for the synaptic plasma membrane.*

Lipid Class	% abundance (soma)	% abundance (synaptic)
PC	40%	36%
PE	23%	30%
PS	4%	6%
SM	4%	3%
PI	8%	6%
Cholesterol	21%	19%

In the considered studies, lipids were separated using thin-layer chromatography and quantified through photodensitometry. This approach allowed for the identification of the lipid headgroups but did not allow for the determination of the specific fatty acid tails within each class. Hence, to determine the relative abundance of specific tails, a review of additional scientific literature was undertaken to create a consensus model. This effort often faced the challenge of sparse data, as some studies reported information on only one acyl chain per headgroup, which complicated exact identification. Thus, we built upon the extensive work carried out in a previous study (Ingólfsson et al., 2017), which reported a coarse-grained computational membrane model that closely approximates the average lipid composition of a mixture of all human neuronal plasma membranes. Although the study authors were aware that different membrane compositions exist for specific cells and cellular regions within the brain, the limited amount of available data led them to construct a model conservatively, which could best represent the average lipid composition of all membranes present in the brain.

Their computational membrane model is the result of an extensive literature review and comprises 15 different lipid classes. Most importantly, the study specified the specific fatty acid tail type for each lipid head group, along with their relative abundance. We thus began by extracting the relative abundances of the tails for each headgroup type from the data reported in Table 1. In greater detail, we first restricted our search to only consider the specific fatty acid tails for which all-atom parameters were validated and publicly available in the CHARMM force field. After recalculating the relative abundances after excluding unparametrized tails, we obtained a simplified representation of the lipid composition relevant to the membranes of interest. This allowed us to construct symmetric membrane models composed of a total of 512 lipids. We decided to only retain the specific phospholipids whose relative abundance was above 2% (i.e., more than 5 lipids per leaflet).

In summary, to investigate how membrane composition influences the structural and dynamical behaviour of computational membrane models, we constructed and compared three distinct membrane types. The first model, adapted as-is from earlier literature (Zizzi et al., 2022), represents an average mammalian cell membrane and serves as a simplified reference. The other two were designed to reflect the specific compositions of neuronal membranes more accurately. To construct these neuronal models, we first determined the relative abundance of the headgroup types using data from in vivo studies of brain tissue. Next, the distribution of specific fatty acid chains for each headgroup family was extracted from a previous study employing a coarse-grained neuronal membrane model (Ingólfsson et al., 2017). The final neuronal soma and synaptic membrane models included: 1,2-dipalmitoyl-sn-glycero-3-phosphocholine (DPPC), 1-palmitoyl-2-oleoyl-sn-glycero-3-phosphocholine (POPC), 1,2-dioleoyl-sn-glycero-3-phosphocholine (DOPC), 1-palmitoyl-2-arachidonoyl-sn-glycero-3-phosphocholine (PAPC) for PC; 1-palmitoyl-2-oleoyl-sn-glycero-3-phosphoethanolamine (POPE) and 1-palmitoyl-2-arachidonoyl-sn-glycero-3-phosphoethanolamine (PAPE) for PE; 1-palmitoyl-2-oleoyl-sn-glycero-3-phosphoinositol (POPI) for PI; and 1-palmitoyl-2-arachidonoyl-sn-glycero-3-phosphoserine (PAPS) for PS. Palmitoylsphingomyelin (PSM), the predominant sphingomyelin type in biological membranes, was also included, along with cholesterol (CHL). The detailed compositions of the neural soma and synaptic membrane models, based on these considerations, are reported in **Tables 6** and **7,** respectively.

Table 6*. Composition of the neuronal soma membrane.*

Lipid	Inner leaflet	Outer leaflet	Total
DPPC	26	26	52
POPC	42	42	84
DOPC	11	11	22
PAPC	23	23	46
POPE	17	17	34
PAPE	42	42	84
PAPS	10	10	20
POPI	21	21	42
PSM	10	10	20
CHOL	54	54	108

Table 7*. Composition of the synaptic membrane.*

Lipid	Inner leaflet	Outer leaflet	Total
DPPC	24	24	48
POPC	38	38	76
DOPC	10	10	20
PAPC	20	20	40
POPE	22	22	44
PAPE	55	55	110
PAPS	15	15	30
POPI	15	15	30
PSM	8	8	16
CHOL	49	49	98

Specifically, we developed two new idealized symmetrical all-atom membrane models, each consisting of a total of 512 lipids designed to better represent the lipid composition of the neuronal soma and the synaptic plasma membrane. While both these models included the same lipid types, their relative abundances are tailored to reflect the distinct characteristics of the soma and synaptic regions, respectively.

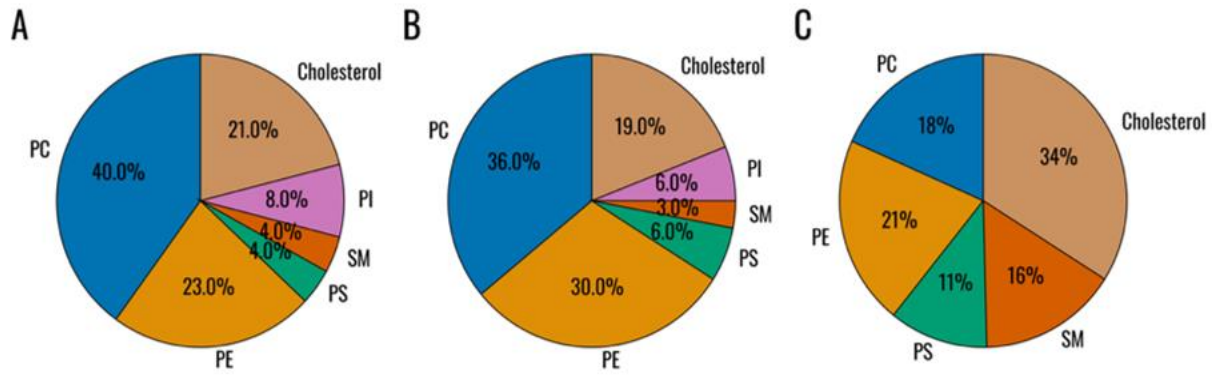

Figure 4. *A: pie chart of the percentage lipid composition of the simplified neuronal soma membrane. B: the pie chart of the percentage lipid composition of the simplified synaptic plasma membrane. C: pie chart of the percentage lipid composition of a composite asymmetrical lipid membrane of a mammalian cell membrane replicated from the work of Zizzi et al. (2022).*

The membranes are built using publicly available and validated molecular mechanics parameters. They were compared to a previously published computational model of an average mammalian cell membrane, featuring a simpler and less heterogeneous lipid composition than the brain-specific models. The molecular models were assembled using the Membrane Builder tool (Jo et al., 2007; Jo et al., 2009; Wu et al., 2014) of CHARMM-GUI (Jo et al., 2008) and parametrized with the CHARMM36 force field (Klauda et al., 2010). To ensure full hydration, membranes were inserted in a rectangular box containing 40 TIP3P water molecules per individual lipid. Na^+ and Cl^- ions were added to reach a physiological salt concentration of 0.15M, and an imbalance was introduced to neutralize the system's net charge. The final composition of each simulated system is shown in **Table 8**.

Table 8*. Components of each simulated membrane system.*

	Lipids	Water molecules	Na	Cl^-	Total molecules
Control	512	61591	99	42	117837
Soma	512	61592	103	41	122384
Synaptic	512	61590	101	41	122588

Acknowledgements

We acknowledge the CINECA award under the ISCRA initiative for the availability of high-performance computing resources and support.

Data availability statement

The datasets and simulation files generated and analyzed during the current study are available from the corresponding author on reasonable request.

Conflict of Interest Statement

The authors declare no conflict of interest.

References

Abraham, M.J., Murtola, T., Schulz, R., Páll, S., Smith, J.C., Hess, B. & Lindahl, E. (2015) GROMACS: High performance molecular simulations through multi-level parallelism from laptops to supercomputers. *SoftwareX* **1–2**, 19–25.

Arriaga, L.R., López-Montero, I., Rodríguez-García, R., Bagatolli, L.A., Monroy, F. & Langevin, D. (2017) Dissipative dynamics of cholesterol-enriched lipid membranes. *Advances in Colloid and Interface Science* **247**,514–520.

Berendsen, H.J.C., Postma, J.P.M., van Gunsteren, W.F., DiNola, A. & Haak, J.R. (1984) Molecular dynamics with coupling to an external bath. *Journal of Chemical Physics* **81**, 3684–3690.

Biasini, M., Bienert, S., Waterhouse, A., Arnold, K., Studer, G., Schmidt, T., Kiefer, F., Gallo Cassarino, T., Bertoni, M., Bordoli, L. & Schwede, T. (2010) OpenStructure: a flexible software framework for computational structural biology. *Bioinformatics* **26**,2626–2628.

Biasini, M., Schmidt, T., Bienert, S., Mariani, V., Studer, G., Haas, J. & Schwede, T. (2013) OpenStructure: an integrated software framework for computational structural biology. *Acta Crystallographica Section D* **69**,701–709.

Calderon, R.O., Attema, B. & DeVries, G.H. (1995) Lipid composition of neuronal cell bodies. *Journal of Neurochemistry* **64**, 424–429.

Chakraborty, S., Doktorova, M., Molugu, T.R., Heberle, F.A., Scott, H.L., Dzikovski, B., Nagao, M., Stingaciu, L.R., Standaert, R.F., Barrera, F.N., Katsaras, J. & Brown, M.F. (2020) How cholesterol stiffens unsaturated lipid membranes. *Proceedings of the National Academy of Sciences of the United States of America* **117**, 21896–21905.

Cordero-Morales, J.F. & Vásquez, V. (2018) How lipids contribute to ion channel function, a fat perspective on direct and indirect interactions. *Current Opinion in Structural Biology* **51**, 92–98.

Cotman, C.W., Blank, M.L., Moehl, A. & Snyder, F.(1969) Lipid composition of synaptic membranes. *Biochemistry* **8**, 4606–4612.

Dias, C. & Nylandsted, J. (2024) Neural membrane repair at the core of regeneration. *Neural Regeneration Research* **19**,1399–1408.

Flyvbjerg, H. & Petersen, H.G. (1989) Error estimates on averages of correlated data. *Journal of Chemical Physics* **91**,461–466.

Grassi, S., Chiricozzi, E., Lunghi, G., Sonnino, S. & Prinetti, A. (2020) Lipid rafts and neurodegeneration: structural and functional roles in physiologic aging and neurodegenerative diseases. *Journal of Lipid Research* **61**,636–654.

Grossfield, A., Patrone, P.N., Roe, D.R., Schultz, A.J., Siderius, D.W. & Zuckerman, D.M., (2018) Best practices for quantification of uncertainty and sampling quality in molecular simulations. *Living Journal of Computational Molecular Science* **1**, 5067.

Hantal, G., Marquardt, D., Vattay, G., Zoni, V. & Róg, T. (2019) Effect of general anesthetics on lipid membranes. *Biochimica et Biophysica Acta (BBA) – Biomembranes* **1861**, 594–609.

Harayama, T. & Riezman, H. (2018) Understanding the diversity of membrane lipid composition. *Nature Reviews Molecular Cell Biology* **19**, 281–296.

Hess, B., Bekker, H., Berendsen, H.J.C. & Fraaije, J.G.E.M. (1997) LINCS: a linear constraint solver for molecular simulations. *Journal of Computational Chemistry* **18**, 1463–1472.

Hess, B., Kutzner, C., van der Spoel, D. & Lindahl, E. (2008) GROMACS 4: Algorithms for highly efficient, load-balanced, and scalable molecular simulation. *Journal of Chemical Theory and Computation* **4**, 435–447.

Humphrey, W., Dalke, A. & Schulten, K. (1996) VMD: Visual molecular dynamics. *Journal of Molecular Graphics* **14**, 33–38.

Ingólfsson, H.I., Melo, M.N., van Eerden, F.J., Arnarez, C., Lopez, C.A., Wassenaar, T.A., Periole, X., de Vries, A.H. & Marrink, S.J. (2017) Computational lipidomics of the neuronal plasma membrane. *Biophysical Journal* **113**, 2271–2280.

Jo, S., Kim, T., Iyer, V.G. & Im, W. (2007) Protein/membrane complexes for MD simulations. *PLoS ONE* **2**, e880.

Jo, S., Kim, T. & Im, W. (2008) CHARMM-GUI: web-based GUI for CHARMM. *Journal of Computational Chemistry* **29**, 1859–1865.

Jo, S., Lim, J.B., Klauda, J.B. & Im, W. (2009) CHARMM-GUI Membrane Builder. *Biophysical Journal* **97**, 50–58.

Johner, N., Harries, D., Khelashvili, G. & Weinstein, H. (2016) Computational analysis of lipid membrane mechanics. *BMC Bioinformatics* **17**, 1–11.

Kao, Y.-C., Ho, P.-C., Tu, Y.-K. & Jou, I.-M. (2020) Lipids and Alzheimer's disease. *International Journal of Molecular Sciences* **21**, 1505.

Klähn, M. & Zacharias, M. (2013) Transformations in plasma membranes of cancerous cells. *Physical Chemistry Chemical Physics* **15**, 14427–14438.

Klauda, J.B., Venable, R.M., Freites, J.A., O'Connor, J.W., Tobias, D.J., Mondragon-Ramirez, C., Vorobyov, I., MacKerell, A.D. & Pastor, R.W. (2010) Update of the CHARMM all-atom additive force field for lipids: validation on six lipid types. *Journal of Physical Chemistry B* **114**, 7830–7843.

Kozłowska, K., Maślanka, T., Wieczorek, M. & Kołodziejczyk, A.(1999) ESR study on melanoma membrane properties. *Experimental & Toxicologic Pathology* **51**, 89–92.

Li, L.B., Vorobyov, I. & Allen, T.W. (2012) The role of membrane thickness in charged protein–lipid interactions. *Biochimica et Biophysica Acta (BBA) – Biomembranes* **1818**, 135–145.

Marrink, S.J., Corradi, V., Souza, P.C.T., Ingólfsson, H.I., Tieleman, D.P. & Sansom, M.S.P., (2019) Computational modeling of realistic cell membranes. *Chemical Reviews* **119**, 6184–6226.

Mesa-Herrera, F., Taoro-González, L., Valdés-Baizabal, C., Díaz, M. & Marín, R. (2019) Lipid and lipid raft alteration in aging and neurodegenerative diseases. *International Journal of Molecular Sciences* **20**, 3810.

Michaud-Agrawal, N., Denning, E.J., Woolf, T.B. & Beckstein, O. (2011) MDAnalysis: a toolkit for the analysis of molecular dynamics simulations. *Journal of Computational Chemistry* **32**, 2319–2327.

Miller, K.W. & Pang, K.-Y.Y. (1976) General anaesthetics can selectively perturb lipid bilayer membranes. *Nature* **263**, 253–255.

Nicholls, A. (2014) Confidence limits, error bars and method comparison in molecular modeling. *Journal of Computer-Aided Molecular Design*, **28**, 887–918.

Nosé, S. (1984) A unified formulation of the constant temperature molecular dynamics methods. *Journal of Chemical Physics* **81**, 511–519.

Park, H. Sut,T.N, Yoon, B-K., Zhdanov,,V.P. Cho,N-J. & Jackman,J.A. (2022) Unraveling how cholesterol affects multivalency-induced membrane deformation of sub-100 nm lipid vesicles. *Langmuir* **38**, 15950–15959.

Parrinello, M. & Rahman, A. (1981) Polymorphic transitions in single crystals: A new molecular dynamics method. *Journal of Applied Physics* **52**, 7182–7190.

Ramos-Martín, F. & D'Amelio, N. (2022) Biomembrane lipids: When physics and chemistry join to shape biological activity. *Biochimie* **203**, 118–138.

Rehberg, B., Urban, B.W & Duch,D.S. (1995) The membrane lipid cholesterol modulates anesthetic actions on a human brain ion channel. *Anesthesiology* **82**, 749–758.

Róg,T. , Pasenkiewicz-Gierula, M., Vattulainen,I. & Karttunen,M. (2009) Ordering effects of cholesterol and analogues. *Biochimica et Biophysica Acta (BBA) – Biomembranes* **1788**,97–121.

Rózsa, Z.B., Flis, A., Ötvös, F., Ujfalusi, Z., Szakács, G., Szabó, G. & Mihály, J. (2023) Understanding the molecular mechanism of anesthesia. *Journal of Physical Chemistry B*, **127**,6078–6090.

Saponaro, A. & Lolicato, M. (2022) Editorial: The key role of lipids in the regulation of ion channels. *Frontiers in Physiology*, **13**,1000082.

Shahane, G., Ding, W., Palaiokostas, M. & Orsi, M. (2019) Properties of biological lipid bilayers. *Journal of Molecular Modeling* **25**, 76.

Sok, M. (1999) Membrane fluidity characteristics of human lung cancer cells. *Cancer Letters* **142**, 17–24.

Song, J. & Waugh, R.E. (1993) Bending rigidity of SOPC membranes with cholesterol. *Biophysical Journal* **64**, 1967–1970.

Tillman, T.S. & Cascio, M. (2003) Effects of membrane lipids on ion channel structure and function. *Cell Biochemistry and Biophysics* **38**,161–190.

Van Der Spoel, D., Lindahl, E., Hess, B., Groenhof, G., Mark, A.E. & Berendsen, H.J.C. (2005) GROMACS: fast, flexible, and free. *Journal of Computational Chemistry* **26**, 1701–1718.

Westra, M., Gutierrez, Y. & MacGillavry, H.D. (2021) Contribution of membrane lipids to postsynaptic protein organization. *Frontiers in Synaptic Neuroscience* **13**, 790773.

Wilson, K.A., MacDermott-Opeskin, H.I., Riley, E., Lin, Y. & O'Mara, M.L. (2020) Understanding the link between lipid diversity and the biophysical properties of the neuronal plasma membrane. *Biochemistry* **59**, 3010–3018.

Wu, E.L., Cheng, X., Jo, S., Rui, H., Song, K.C., Davila-Contreras, E.M., Qi, Y., Lee, J., Monje-Galvan, V., Venable, R.M., Klauda, J.B. & Im, W. (2014) Realistic biological membrane simulations. *Journal of Computational Chemistry* **35**, 1997–2004.

Xie, P., Su, Z., Zhang, W. & Zhang, L. (2023) Membrane proteins and membrane curvature: Mutual interactions and a perspective on disease treatments. *Biomolecules* **13**, 1772.

Yoon, J.H., Kim, H.Y., Moon, M.H. & Lee, J.W. (2022) Brain lipidomics: From functional landscape to clinical significance. *Science Advances* **8**, eadc9317.

Zizzi, E.A., Lin, L., DiNuzzo, M., Matsumoto, S., Green, J.J. & Eckenhoff, R.G. (2022) Alteration of lipid bilayer mechanics by volatile anesthetics. *iScience* **25**, 103946.